Novel Use of a Hand-Held Laser Induced Breakdown Spectroscopy Instrument to Monitor Hydride Corrosion in Uranium

E. Garlea[1,*], B. N. Bennett[1], M. Z. Martin[2], R. L .Bridges[1], G. L. Powell[1] and J. H. Leckey[1]

[1] CNS/Y-12 National Security Complex, Development Division, Oak Ridge, TN 37831, USA

[2] Oak Ridge National Laboratory, Biosciences Division, Oak Ridge, TN 37831, USA

*Corresponding Author: garleae@y12.doe.gov

ABSTRACT

Using a compact hand-held laser-induced breakdown spectroscopy (LIBS) instrument, studies were conducted on specimens of uranium charged with controlled hydrogen concentrations for a qualitative evaluation of hydride corrosion. Four samples of depleted uranium with two different starting microstructures (cast and rolled) were used for this study. The hydrogen charged samples (rolled 1.8 wppm H and cast 14 wppm H by weight) are representative of the pre-corrosion states with hydrides distributed throughout the bulk. In-depth LIBS measurements were carried out, after the thick surface corrosion layer was removed, by applying 100 laser pulses from sample surface into the bulk on five different sample locations. Three additional areas on each sample were studied by laser ablation using a 12-point grid approach. The atomic emission signals of elemental uranium, carbon, hydrogen, and oxygen were identified and analyzed. All four samples showed similar uranium and carbon concentrations, as expected. Hydrogen content was consistent with each sample's specification, such that the hydrogen charged samples exhibited higher hydrogen concentration than their references. Both specimens charged with hydrogen showed elevated oxygen content as well, due to rapid oxidation of uranium and uranium hydrides. The oxidation process was facilitated by the laser ablation and plasma plume's high temperature effects on the sample combined with the glovebox environment. The uranium surface damage produced by laser ablation was quantitatively evaluated by optical microscopy.

Keywords: uranium; surface damage, hydrogen embrittlement; hydride corrosion; laser-induced breakdown spectroscopy; hand-held LIBS.

1. BACKGROUND

Uranium hydride corrosion has been extensively studied to understand the mechanisms of formation and its effects on the uranium matrix [1], [2], [3], [4], [5], [6]. It is believed that the early stages in metal processing are susceptible to hydrogen contamination, placing the metal in a pre-corrosion state, with UH_3 precipitates formed and distributed throughout the bulk. Upon subsequent hydrogen exposure, the precipitates can grow to fully developed corrosion sites. Corrosion initiation sites are directly related to the properties and characteristics of the uranium metal lattice such as grain boundaries and twinning. However, defects and inconsistencies in the overlaying oxide layer are the pathway for environmental hydrogen to diffuse into the uranium bulk. Dislocations have high affinity for interstitial hydrogen and provide a very efficient transport mechanism. The most studied phase is the β-UH_3 phase, named in general as the uranium hydride. Under certain conditions of temperature and pressure, the α-UH_3 phase could form, but a pure sample of α-UH_3 bulk has not yet been obtained.

When formation of hydrides has significant implications on the microstructure and mechanical behavior of uranium, the phenomenon is called hydrogen embrittlement. Hydrogen embrittlement appears to occur even with the addition of relatively low amounts of hydrogen. For example, approximately 50% decrease in ductility was observed at hydrogen contents of 0.35 wppm [1]. Enhanced crack nucleation and crack propagation are most common features of hydrogen embrittlement, with hydrogen having high diffusivity in the region of stress at the crack tip, also known as a stress enhanced mechanism [7] [8]. Moreover, the fracture mechanism can change from ductile rupture to brittle intergranular decohesion without affecting the bulk plastic deformation [9].

In the presence of hydrogen gas at elevated temperature, uranium absorbs hydrogen as an interstitial solute and UH_3 is formed upon cooling. The cooling rate has a direct effect on the morphology of hydrides; as such fast cooling (e.g. water quenching) produces finely dispersed particles difficult to be observed microscopically [7].

Uranium corrosion is a very complex and challenging process that originates from the competing corrosion species such as oxygen, hydrogen, and as well as H_2O. These corrosion elements have different interactions and effects on uranium, based on their form and environment [10], [11]. While very small amounts of hydrogen embrittles uranium, absorbed oxygen behaves as an interstitial solute in uranium competing with hydrogen for the capacity of the metal to solvate interstitials [7]. The high affinity of uranium for oxygen adds an additional challenge to the characterization of hydrides.

Laser-induced breakdown spectroscopy (LIBS) is a candidate technique for characterization of nuclear materials, although there is not an abundance of articles on the subject. As a surface investigative technique, LIBS has been used for the detection of uranium in liquids for nuclear reactor fuel reprocessing [12], the detection of impurities in uranium related to reactor nuclear fuel production [13] [14], and the detection of aerosols containing uranium [15]. A comprehensive report from Los Alamos National Laboratory shows the LIBS spectral data for mixed actinide reactor fuel pellets and details the specific peaks in the wavelength range of 200-780 nm [16]. Thus far, LIBS has been used to identify uranium and other nuclear elements in solid pellets [13], [17] [18], metals [19], in solutions [12], and dried on substrates such as filter paper [20]. LIBS is also a versatile tool for isotopic analysis of nuclear materials [20] [21] and for understanding actinide plasma chemistry [22].

A complex study in terms of instrument development of LIBS for uranium detection at close and standoff distances has been done by Chinni et al. in 2009 [23]. Furthermore, Cremers, et. al. in 2012 developed a field-deployable instrument to monitor in-field radiological, nuclear, and explosive threats to screen suspect facilities [20]. In particular, this person-portable LIBS probe was used to determine the limits of detection for impurities such as Al, Ca, Cr, Cu, Mg, Na, and V in U_3O_8 samples. This article also reported the LIBS spectra of hydrogen and deuterium detected from water and heavy water that was deposited on glass microfibers. In 2013, the LIBS technique was used for depleted uranium, thorium powders, and uranium ore as a potential rapid in-situ analysis technique in nuclear reactor production facilities, environmental sampling, and in-field forensic applications [24]. The influence of ambient gas in the detection of uranium metal was also reported. Argon was observed to be the best ambient atmosphere for the detection of uranium emission lines [25]. Studies showed that the hydrogen Balmer emission line intensity

from sample surface, and from within the sample, can be differentiated such that the hydrogen from the surrounding environment decreased, and the hydrogen from bulk of the material increased as the measurement continued [26].

Generally, LIBS has been represented as an analytical surface technique, but it has also been shown that LIBS can be used for depth profiling of a sample. For depth profiling, the laser beam is focused onto the surface of a sample and held at the same position for a certain number of laser pulses to ablate the material. This approach has been employed for the current study.

In this paper, a systematic and detailed study using a hand-held LIBS instrument (HH LIBS) has been conducted aiming to:

- Identify the presence of hydrogen, oxygen, and carbon within the uranium bulk samples in a glovebox.
- Compare qualitatively the corrosion products in the two samples with different hydrogen concentration to evaluate corrosion.
- Evaluate the surface damage produced by laser ablation via microscopy.

2. EXPERIMENTAL DETAILS

2.1 Samples and Hydrogen Charging

Four samples of depleted uranium (DU) with two different starting microstructures were used for this study to monitor the corrosion process. Two samples were kept in as-received conditions as the reference, and a sample representative of each microstructure was charged with a known amount of hydrogen, Figure 1. The rolled microstructure was charged to 1.8 wppm hydrogen, while the cast microstructure was charged to 14 wppm hydrogen. The hydrogen concentrations were achieved by varying the temperature and time of charging but keeping the hydrogen partial pressure constant. Ref. [1] provides references and details of the hydrogen charging thermodynamic process and how the partial pressure of hydrogen can be used to control the amount of hydrogen intake by the sample. Briefly, the concentration of hydrogen, $[H]_U$,

dissolved in uranium at equilibrium is proportional to the square root of partial pressures of hydrogen, P, following Sievert's law:

$$[H]_U = k_s(T)P^{0.5} \quad (1)$$

where $k_s(T)$ is a temperature-dependent constant of proportionality, also known as the Sievert's parameter. To charge samples with controlled amounts of hydrogen a combination of annealing/outgassing and hydrogen charging processes take place. The outgassing process consists of annealing the sample at a constant temperature in high vacuum with the main goal of removing the existing hydrogen from the bulk to yield a 0 wppm condition. Then, while keeping the temperature constant, a known volume of high purity (99.9999%) hydrogen gas is introduced in a closed system to produce the desired pressure. The charging process is followed by a rapid water quench of the sample to precipitate the formation of hydrides. The 1.8 wppm sample underwent a 3-hour annealing at 630 °C and a 3-hour charging at 630 °C under hydrogen gas. For the 14 wppm sample, a 2-hour annealing at 850 ºC was followed by a 2-hour hydrogen loading at 850 ºC. The hydrogen contents of these two samples were not directly measured for the current study. Rather, the hydrogen content was calculated using the method described in reference [1] or by similar embrittlement behavior observed at a specific charging level, providing evidence in support of this assumption [1] [9]. The hydrogen charged samples mimic the pre-corrosion conditions with hydride precipitates distributed throughout the sample's bulk.

The starting rolled microstructure has the average grain size approximately 25 μm, Figure 1 (a), while after the charging process it was observed a prevalent distribution of small grains and much larger grains with grain diameters averaging close to 550 μm. The rolling processing history was documented in other publications [9], [27] [28]. The as-cast microstructure, Figure 1(b), depicts a typical mixed grain size, ranging from centimeter to micrometer length scale similar to that reported in [29], while after the charging process some reduction in grain size is noticeable. It is noted that both starting microstructures had the same casting protocol and specifications. The presence of hydrides was not expected to be observed by microscopy in the hydrogen charged microstructures, because the water quenching yielded too fine precipitates for identification by this technique.

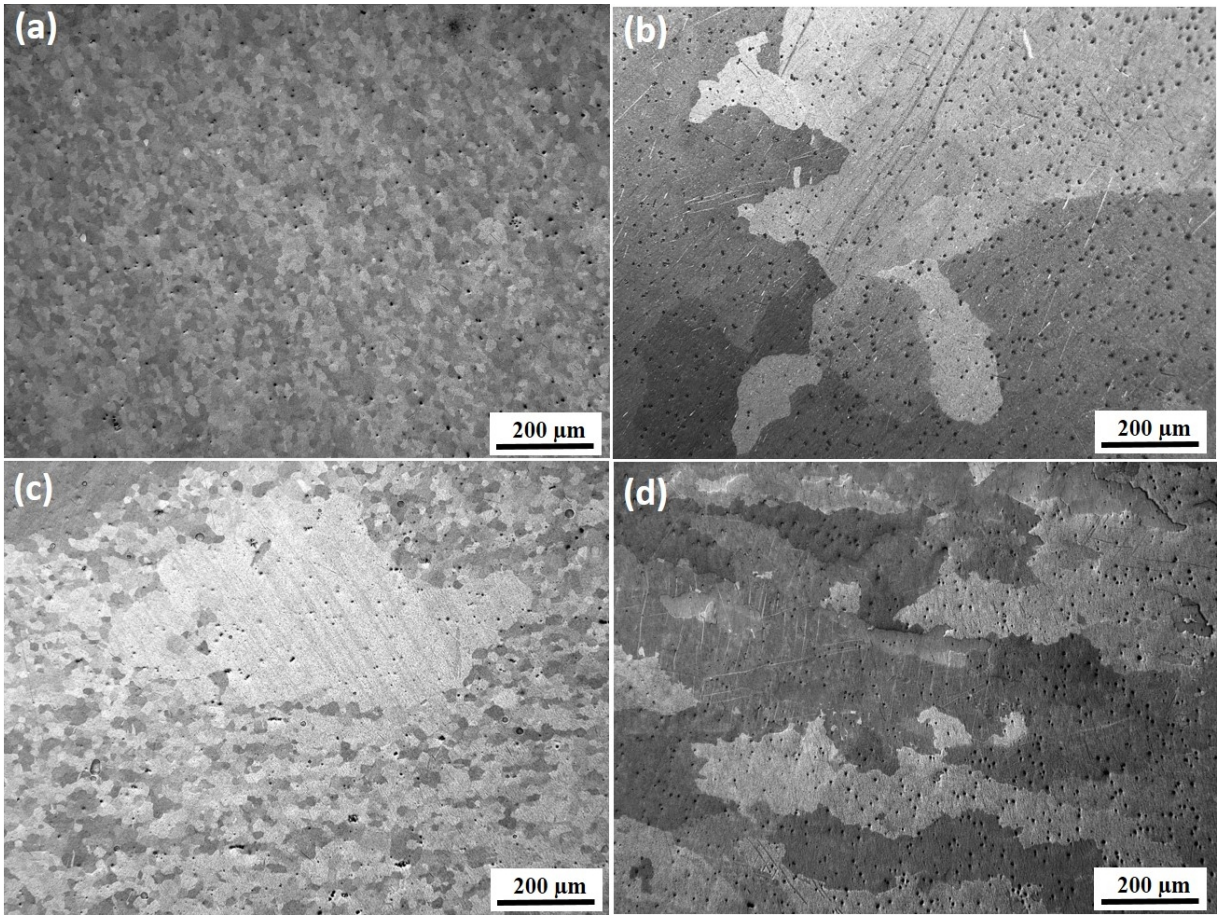

Figure 1. Optical micrographs showing the starting microstructures for a) as-rolled and b) as-cast cases; the resulting microstructures after hydrogen charging for c) rolled 1.8 wppm H and d) cast 14 wppm H samples.

2.2 HH LIBS Measurements

The four samples were mounted in metallographic mounts of epoxy and mechanically polished. Note that the two hydrogen charged samples were removed from larger cylinders after the charging process, to ensure that LIBS samples are representative of bulk the pre-corrosion state. A final milling to remove the oxide layer was done using a Gatan PECS II Model 685 ion polishing system. Each sample surface was milled for a duration of 2 hours at 8 KeV inside an argon gas atmosphere with the guns tilted at 8°. The samples were then quickly moved (few minutes) to a glovebox with argon atmosphere. Using the HH LIBS instrument, two sets of measurements were carried out, consisting of an in-depth strategy and a 12-point grid strategy.

The testing details are summarized in Table 1. For the in-depth strategy, 100 laser pulses total were applied continually as shown in the following protocol: every 10 laser pulses were automatically applied, 1 laser pulse at a time at a rate of 10 Hz between pulses. The 10 spectra collected are automatically averaged randomly by the software resulting in one spectrum. There is a break of 1-2 seconds (sec) between each set of 10 laser pulses, which was the time needed to press the instrument's start button. Then, the next 10 laser pulses are activated, which are averaged again to one spectrum. Therefore, the averaging yields 10 spectra per sample location as the laser ablates the sample from its surface into the bulk. This in-depth measurement was done on five different locations for each sample. As indicated in Table 1, prior to in-depth data collection, there is a cleaning shot performed when no data are collected. For the 12-point grid strategy, the laser automatically ablates 12 different spots on the sample in a certain pattern at 400 μm intervals between the centers of adjacent spots. More details about the 12-point grid specifics are available in Ref. [30]. For each one of the 12 spots, there are 3 laser pulses collected that result in 36 spectra, which are automatically averaged onto one spectrum. Three different areas on each sample were studied using the 12-point grid. Before the 12-point grid data collection occurred, there were 20 cleaning shots without collecting the data, resulting in a 23 laser pulses depth. This was done to ensure the sample laser penetrated the surface and collected data are representative of the bulk. Figure 2 shows a schematic of the laser strategies employed. The in-depth 100 laser pulses in 5 different locations are marked by individual circles, whereas the 12-point grid in 3 different locations are marked by the group of 12 circles. These measurements were grouped by the strategy to avoid overlapping, such that the microscopy study could be carried out after the LIBS tests were done.

The Z-500 instrument HH LIBS instrument from SciAps, Inc. [31] was used which contains a solid-state laser system operating like a class I laser. More details about the use of Z-500 instrument have been recently reported [32] [30]. For example, using the same instrument, elements in sub-percent level were identified and calibration curves were produced [30]. Specifically, this instrument has an incident wavelength of 1532 nm, a laser energy of 5 mJ per pulse, a pulse duration of 5 ns, operates at a repetition rate of 10 Hz, and is equipped with argon gas purging capability. Argon gas was flushed through the sample window for 3 seconds before each spectrum was collected, although the measurements were carried out in a glovebox. The spot

size of the laser ablation on the sample surface is 40 µm. Integration period and integration delay used for this study were 250 nsec and 650 nsec, respectively.

Table 1. Testing parameters employed for the HH LIBS instrument to investigate uranium samples in a glovebox.

HH LIBS test set up	*1 point: in-depth ablation*	*12 point grid - laser*
Number of test sample locations	5 areas	3 areas
Number of cleaning pulses	1	20
Number of laser pulses	1	3
Number of pulses per location	100	36 (3 x 12)
Number of pulses to average	10 for 100 pulses per location	36 per location
Averaging method	Random	Random
Argon preflush (msec)	3000	3000
Integration period(nsec)	250	250
Integration delay (nsec)	650	650
Test rate (Hz)	10	10
Clean rate (Hz)	10	10

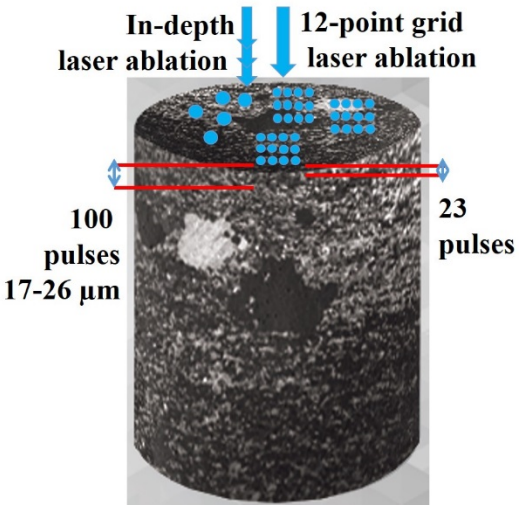

Figure 2. Schematic of 1.8 wppm H sample showing the ablation strategies employed. The five in-depth locations for 100 laser pulses are marked by single circles. Each of the three 12-point grid areas are marked by a group of 12 circles. Schematic not drawn to scale.

A Keyence VHX - 2000 digital microscope was used to study the surface damage created by the laser. The microscope uses white light and focus variation to acquire in-depth (height) data for three dimensional representation of surface damage. The depth algorithm is based about each pixel finding optimal focus and then tracking the height through the mechanical height (z) motor. An in-depth measurement was conducted and three-dimensional images were reconstructed to provide the diameter and height of the craters formed from the laser ablation. Only craters formed from the in-depth laser ablation for 100 laser pulses were studied. The quantitative results are presented as the average values and the standard deviation is included.

3. EXPERIMENTAL RESULTS

Figure 3 (a) shows examples of three spectra collected in a glovebox using the HH LIBS on the rolled sample containing 1.8 wppm H on one location. During the 100 laser pulses ablation, data are averaged every 10 pulses, and therefore the three spectra shown are representative spectra from the sample's surface (first 10 pulses), mid-depth (50 pulses), and after 100 laser pulses deep in the sample's bulk. Prominent peaks are observed for the argon that is pumped on the sample surface from the LIBS instrument and from the argon atmosphere in the glovebox. These argon peaks are identified as 696.543, 706.722, 738.398, 750.387, 751.465, 763.511, 772.376, 794.818, 800.616, and 801.479 nm. Additionally, the spectra were studied for several peaks of interest, such as oxygen peak at 777.194 nm, hydrogen peak at 656.279 nm, and carbon peak at 193.091 nm, Figure 3 (b). It is acknowledged that there are multiple peaks for uranium, however, only the uranium peak at 591.539 nm, which was very well defined, was studied here. The background baseline of spectra from different measurements are similar (i.e., similar *bremsstrahlung*). Although carbon is not a direct corrosion element, it had been reported that carbides may serve as a pathway for hydrogen diffusion in the metal, thus carbon plays a role in the hydrogen embrittlement process [33] [34]. Carbon content investigation was also part of evaluating the instrument's capability to probe elements at the margin of the spectrum that are present in small amounts in the material. When Figure 3 (a) is enhanced to exclude the argon peaks, many elemental peaks become more visible with U peak at 591 nm and C peak at 193 nm marked, Figure 3 (c). The large step observed around 420 nm is an artifact specific to this instrument and it is not related

to the material studied. The same step is observed in copper and aluminum alloys studies reported by the same authors in Ref. [30].

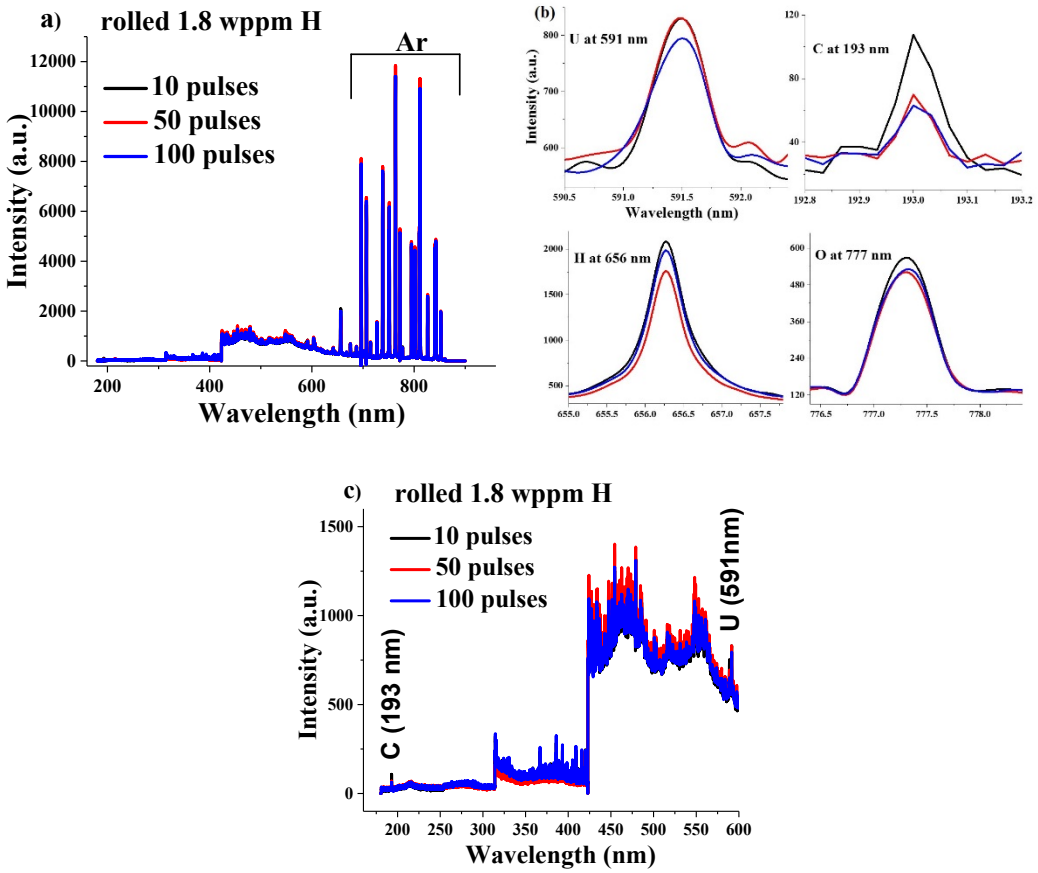

Figure 3. HH LIBS spectra collected on the rolled 1.8 wppm H uranium sample (a) from the sample's surface (10 laser pulses) to the 100 pulses in depth; (b) zoomed in peaks for uranium peak at 591.539 nm, carbon peak at 193.091 nm, hydrogen peak at 656.279 nm, and oxygen peak at 777.194 nm; (c) zoomed in spectra to 600 nm.

H concentration effect

For a qualitative analysis of spectra, the peak intensity for each element of interest was corrected by subtracting its background (value taken at the flattest wavelength in peak's vicinity). Figure 4 is a comparison of corrected peak intensity variation with the number of laser pulses from the sample's surface into the bulk for all four samples. Each data point (10 spectra interval) in the graph is an average of the 5 locations for the in-depth study and the standard deviation included is

determined from the 5 spectra/data point. In addition, the results from the 12-point grid study are also plotted as a symbol and are annotated by "grid" in the legend of each graph. The grid data is equivalent to 20 laser pulses into the samples, since there were 20 cleaning pulses employed. The grid results and standard deviations are obtained from the average of the three different areas studied, consisting of an average of 108 spectra total.

The four elements examined have similar trends in all cases. In the case of hydrogen, consistently, its signal intensity drops significantly once the first 20 laser pulses are ablated and then follows a linear trend for the rest of 80 laser pulses for all four samples. This could be due to the imminent formation of the thin passivation corrosion layer and environment effects before the laser fully penetrates the bulk. For the rolled samples, as-rolled and rolled 1.8 wppm H, the grid data for H are in close agreement with the in-depth data. Somewhat slightly lower values for the grid results can be observed, especially for rolled 1.8 wppm H. Furthermore, the grid results for H for the cast samples, Figure 4 (b and d) are more significantly lower than the in-depth data. This disagreement could be due to the larger grain size and sample inhomogeneity. However, there has not been a systematic statistical variation in the obtained results to lead to a definitive conclusion in regard to the effect of the grain size and microstructure on the LIBS data for this study. For the LIBS technique, the particle size is important because the plasma conditions, such as plasma temperature, are dependent on the size of particles, and these effects must be corrected to obtain quantitative information. There was observed up to 50% emission signal enhancement on LIBS measurements for most elements by improving particle size distribution and consequently the pellet porosity [35], [36].

The other three elements, U, O, and C, exhibit a linear trend in the scale range used for in-depth study, and these results overlap with the 12-point grid results at data point 20.

It can be seen [note same Y- scale for both Figures 4 (a) and (b)] that overall peak intensities for all four elements are noticeably consistent in both reference samples. When comparing Figures 4 (c) and (d), it is observed that there is a far greater hydrogen response for 14 wppm H sample than the 1.8 wppm H sample, as it was expected. An increase is noted in oxygen intensity in the 14 wppm H sample, which confirms the sample with a higher amount of hydrogen has a greater level of corrosion. The carbon and uranium peaks are noticeably consistent in both samples. At the integration delay of 650 nsec used for this study, only the ionic and atomic peaks

are detected. However, recent studies, employing a larger time scale in the 10s of microsecond range, allow detection of molecules, such as uranium monoxide for example [22] [37].

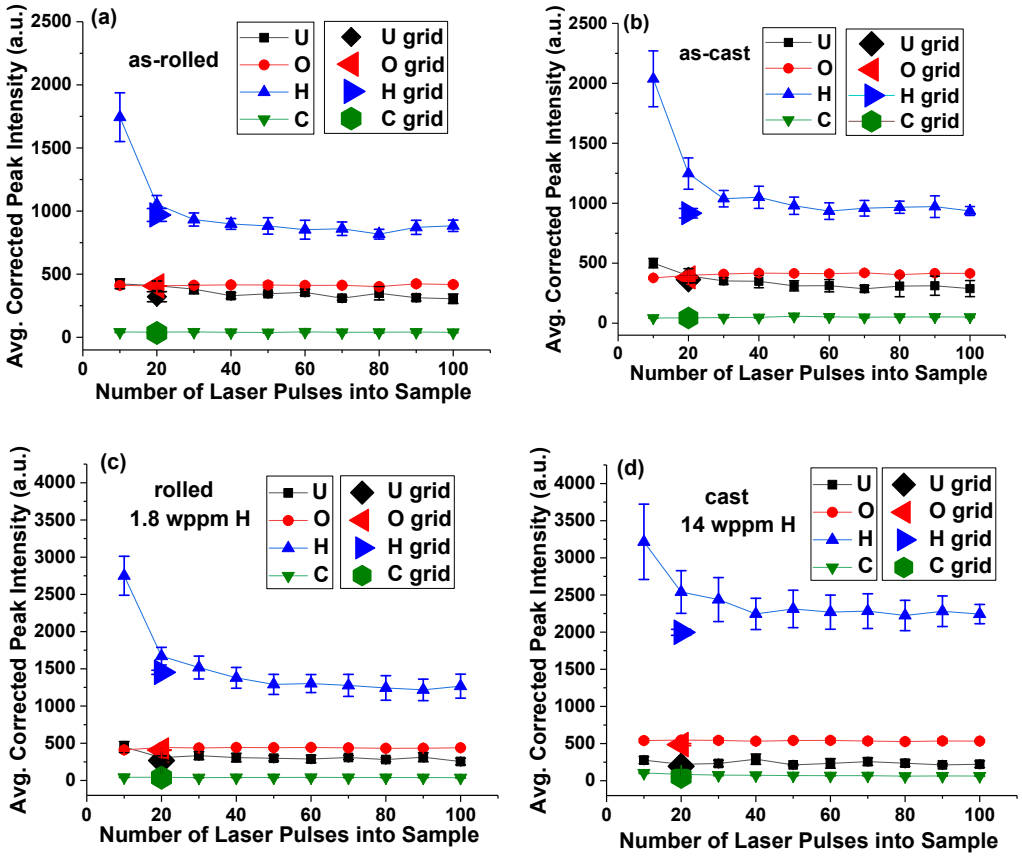

Figure 4. Comparison of averaged corrected peak intensities for U, H, O, and C that were identified in the a) as-rolled and b) as-cast samples; c) rolled 1.8 wppm H and d) cast 14 wppm H samples. Data are plotted as a function of laser depth penetration from the surface for 100 pulses with every 10 pulses averaged. All five in-depth locations are averaged. The data from the 12-point study are plotted as well, as an average of the three areas measured.

Corrosion Effects

The elemental comparison of all samples studied are presented at more sensitive scales in Figure 5, with the absolute standard deviation included for each data point. Results are included

for both laser ablation strategies, in-depth and 12-point grid. The uranium data profiles for all four samples, Figure 5 (a), are overall similar within the error bar, especially after 40 laser pulses in the bulk. This is to be expected since the matrix consists of uranium metal, and uranium being the major component for all samples should be similarly detected with this technique. At data point 20, the 12-point grid results are in good agreement with the in-depth data and the overall data scattering is approximately 200 a.u.

Nevertheless, carbon, oxygen, and hydrogen are minor elements in the uranium matrix. It is not fully understood why carbon intensity, Figure 5 (b), for the cast 14 wppm H sample is consistently decreasing for the first 50 laser pulses into the sample instead of following a linear trend such as the other three samples. It is noted the cast 14 wppm H exhibits the highest C peak intensity, followed by the as-cast condition. The rolled samples have almost the same elemental variation in C within the bulk. Even though for the first 50 laser pulses the 14 wppm H sample has elevated peak intensities, when looking at the 12-point grid results in Figure 5 (b), there is only approximately 35 a.u. variation amongst the samples, excluding the in-depth data for the 14 wppm H samples.

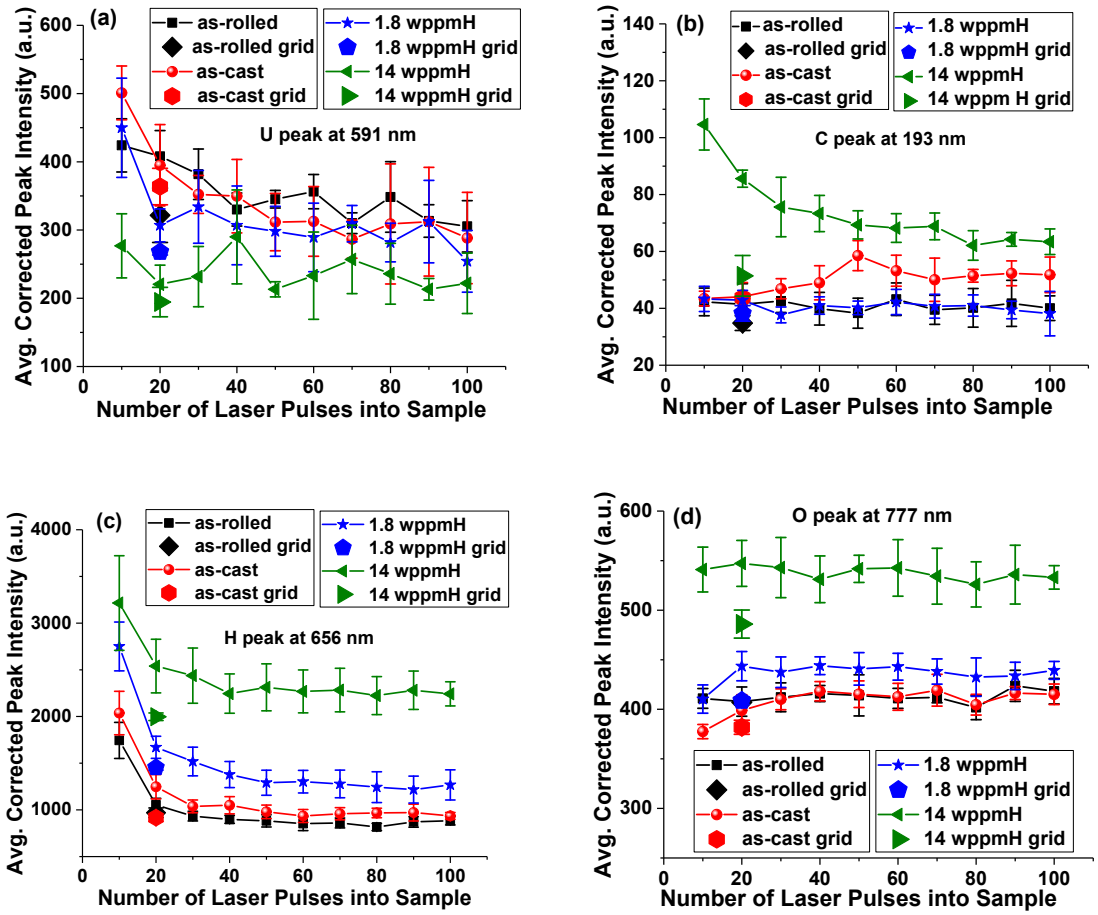

Figure 5. Comparison of atomic emission signals for the four samples studied by 100 laser pulses and 12-point grid: (a) uranium at 591.539 nm, (b) carbon at 193.0905 nm, (c) hydrogen at 656.279 nm, and (d) oxygen at 777.194 nm.

To depict the corrosivity within the sample, oxygen and hydrogen are measured at higher and lower amounts within the 14 wppm H and 1.8 wppm H samples, respectively, as they compare to the as-received conditions in Figure 5 (c). Comparing first the as-received cases, the as-cast sample exhibits almost slightly higher signal for H. When looking at the 12-point grid results, which consists of an average of 108 spectra, the as-rolled sample has a slightly higher H atomic emission signal. Higher hydrogen concentration in the as-rolled case than in the as-cast sample is sometimes expected due to the additional rolling and annealing steps this sample underwent, which can trap more hydrogen in the bulk [5].

As predicted, sample rolled 1.8 wppm H has more hydrogen than its reference, as-rolled, while the 14 wppm H has the highest hydrogen concentration. It is noted that this is a qualitative comparison of the hydrogen peak intensities, and the differences observed between samples are not quantitative.

In the case of oxygen, Figure 5 (d), the cast 14 wppm H sample exhibits the highest emission signal, followed by the rolled 1.8 wppm H sample. The lowest concentration of O is present in the reference cases, as-rolled and as-cast samples, which depict the same peak intensity. The grid results for O are lower than the in-depth results, similarly with elemental H. Again, the grid data suggest a higher concentration in O for the as-rolled sample than the as-cast, which can be expected, due to the rolling processes that many times can trap O and H in the bulk. The presence of hydrogen and oxygen at higher intensities are indicative of more corrosion being present in the 14 wppm H sample than in 1.8 wppm H.

Laser surface damage evaluation

Figure 6 shows three-dimensional representation of the craters, in a cone shape, produced in the case of (a) rolled 1.8 wppm H, (b) cast 14 wppm H, (c) as-rolled, and (d) as-cast cases from the 100 laser pulses, measured using high-resolution microscopy. These images are presented as examples. To quantitatively evaluate the surface ablation, a line profile measurement available in the Keyence software was used to determine the cone's dimensions, as visible by the red line overlapped on each image. The values obtained are summarized in Table 2, representing the crater size, and the standard deviation for each dimension is included. It is evident that these numbers are not absolute numbers since they rather depend on the sampling location. However, the same selection was applied to all four samples consistently. It is believed that somewhat the microstructure plays a role on the size of the crater. Overall, the two samples with smaller grain size, as-rolled and rolled 1.8 wppm H, exhibit craters approximately 17 μm and 19.5 μm deep. It was observed that the cones for as-rolled sample, varied from being sharp and tall to wide and short, resulting to an average of 17±3 μm. As a comparison, the as-cast crater is 26±4 μm in depth. A height of 22±5 μm was obtained for the cast 14 wppm sample. Slightly taller cones for the cast samples than the rolled samples were seen. However, more studies on the surface damage evolution are needed for a consistent evaluation of the grain size effect.

Because of the melting and rapid cooling of the sample and extensive surface damage, it was challenging to accurately measure the ablation's diameter, the base of the cone. The averaged diameter varies from 44 to 37 µm, when the laser diameter is 40 µm, therefore, the crater diameter should be at least that size.

Table 2. A qualitative summary of depth penetration (crater's height) and crater's diameter produced on the uranium samples by 100 laser pulses.

Sample Name	*Depth of Laser Ablation (µm)*	*Diameter of Laser Ablation (µm)*
ROLLED 1.8 WPPM H	20 ± 3	44±4
CAST 14 WPPM H	22±5	40±4
AS-ROLLED	17±3	37±5
AS-CAST	26±4	37±4

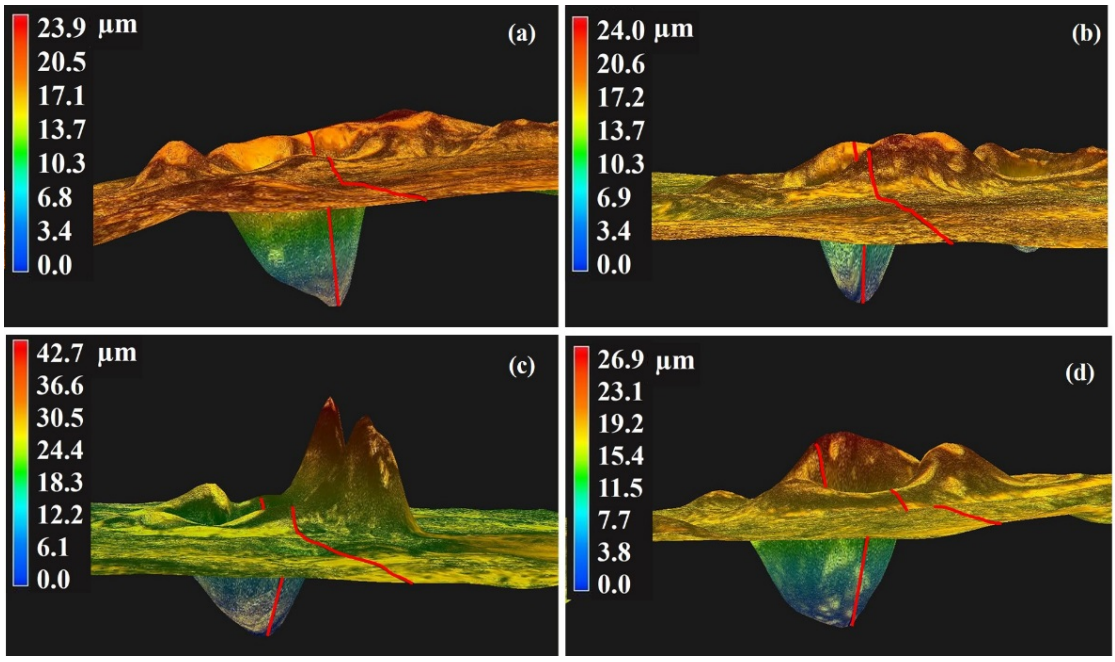

Figure 6. A representation in three-dimensions of surface damage from 100 laser pulse ablation with the line profile overlapped on the images for: (a) rolled 1.8 wppm H, (b) cast 14 wppm H, (c) as-rolled, and (d) as-cast samples.

4. DISCUSSION

It is known that the LIBS laser ablation profiles are exceedingly unique to the samples under investigation and vary based on material properties and experimental protocols [38], [39]. In this case, a novel LIBS approach consisting of a small compact hand-held instrument was used to investigate the uranium corrosion in two samples charged with different hydrogen concentrations and thus different states of pre-corrosion. The measurements were conducted from the sample's surface into the bulk for 100 laser pulses on 5 different locations for each sample. A 12-point grid strategy was also employed at a depth of 20 laser pulses into the bulk, and 3 laser pulses were applied for data collection. The 12-point grid allowed the collection and averaging of 36 spectra per test location, resulting in a final average of 108 spectra.

The technique captures well the differences in the atomic emission signals for four elements, as these signals pertain to the elemental composition. Overall, all four samples show similar concentration of uranium, as expected, since uranium is the matrix element.

In the case of measured elemental carbon, all four samples show consistency, especially the grid results. The 14 wppm H sample suggests an unexplained elevated C content for the first 50 laser pulses in the bulk, however, for the last 50 pulses into the bulk, all four cases have a similar profile within the error bar.

For hydride corrosion, the HH LIBS technique was used to monitor differences in elemental corrosion species (hydrogen and oxygen) amongst the samples. The hydrogen intensity follows the expected trend with the lowest values observed for samples in the as-received conditions (as-rolled and as-cast) and the highest intensity for the 14 wppm H sample. The rolled 1.8 wppm sample has more hydrogen in the bulk than the as-rolled reference sample, as predicted. The intensity variation for oxygen, a function of the oxygen concentration measured in each sample, is more complex and is believed to be specific to the corrosion of uranium hydrides. All four samples show the presence of oxygen in the bulk, with the cast 14 wppm sample exhibiting significantly more O than the other three samples, whereas the 1.8 wppm case has a higher O content than its reference. Likewise for the case of elemental hydrogen, the reference samples have a very similar O concentration. The goal here is to explain the increase in oxygen concentration for the cast 14 wppm H sample and rolled 1.8 wppm H. To understand the results, the laser induced

plasma plume's temperature and its effect on the sample need to be taken into consideration in the context of glovebox environment. The glovebox atmosphere includes moisture and oxygen gas (O_2), among other environmental species. During formation of plasma plume, the temperature is above 4500 °C [21], promoting a dehydrogenation in all samples, thus the hydrogen concentration profiles observed (Figure 5 (c)). As the laser ablates the sample, fresh uranium surfaces are exposed to the humid environment of the glovebox, undergoing a rapid oxidation following equation (2) [5]. In the case of the cast 14 wppm sample, with the highest hydride density, after dehydrogenation/dehydriding, the uranium metal is left with even a higher affinity for oxidation. In addition, the hydrides freshly exposed to the glovebox environment react directly with the humidity through equation (3) [5] or with the oxygen gas through equation (4) [40]:

$$U(s) + 2H_2O(l) \rightarrow UO_2(s) + 2H_2(g) \quad (2)$$

$$2UH_3(s) + 4H_2O(l) \rightarrow 2UO_2(s) + 7H_2(g) \quad (3)$$

$$3UH_3(s) + 25/4\ O_2\ (g) \rightarrow U_3O_8(s) + 9/2H_2O(v) \quad (4)$$

Oxidation of hydrides in argon/oxygen atmosphere had been reported as an accepted approach to "passivate" hydrides for a safe handling of spent fuel plates, as hydrides were present in the corrosion products of severely corroded plates [41] [42] [40]. Therefore, the highest oxygen concentration in the cast 14 wppm sample is due specifically to the oxidation of hydrides. The oxidation process of fresh uranium and uranium hydrides is favored by the high temperature plasma formation followed by rapid cooling of plasma during optical emission. The LIBS repetition rate of 10 Hz between laser pulses and a laser pulse width of 5 nsec yield cooling to take place instantaneously [39] [43]. Even more, there are about 1-2 seconds between each set of 10 laser pulses (each data point in Figures 4 and 5) which means that the plasma is dissipated. However, as seen in the images in Figure 6, there is observable extensive heat damage on sample surface beyond the cone's base. The extensive heat damage occurrence is also supported by Equation (4). It is known that UH_3 is very pyrophoric and can easily burn even at room temperature following the reaction in equation (4). This reaction releases a significant amount of heat, reportedly about 1490 KJ/mol UH_3 [40]. Therefore, this exothermal heat added to the rapid heating-

cooling process during laser ablation, produces the observed surface damage facilitating the oxidation of freshly exposed uranium and uranium hydrides to the environment.

The rolled 1.8 wppm sample has a lower oxygen concentration than the 14 wppm sample, in agreement with the lower hydrogen concentration (fewer hydrides), thus less oxidation. The 1.8 wppm of hydrogen represents about 257 vol. ppm UH_3 vs. 1,995 vol. ppm UH_3 for the 14 wppm case.

CONCLUSIONS

A fundamental study was conducted using a small HH LIBS instrument to detect and characterize corrosion within uranium metal. Samples in as-rolled and as-cast conditions were used as the starting reference samples. Controlled hydrogen charging produced two samples with different microstructures and hydrogen content, rolled 1.8 wppm H and cast 14 wppm H, to mimic two pre-corrosion states. For each sample, five different locations were measured in-depth for 100 laser pulses. Using a 12-point grid approach, HH LIBS data were collected on three additional locations for each sample, at a depth of 20 laser pulse in the bulk. The depth profiles of the corrosion elements, hydrogen and oxygen, have been shown for all four specimens from the surface of the sample into the bulk. The atomic emission signals for hydrogen and oxygen were systematically highest for the 14 wppm H sample, followed by the 1.8 wppm H, and then the reference samples. The elevated content of oxygen in the hydrogen charged samples originates from the oxidation of uranium metal and uranium hydrides during the LIBS measurements, facilitated by the temperature effect on the sample from the laser induced plasma plume combined with the glovebox environment. While the hydrogen concentration followed the expected trend since these samples were intentionally charged with known amounts of hydrogen, the oxygen concentration followed the same trend, indicative of the strong correlation between internal hydrogen content and corrosion.

Additionally, variation of uranium and carbon was monitored and overall showed similar content.

Quantitative evaluation of the surface damage produced by the laser ablation indicated that there is a cone shape damage with a maximum of approximately 26 µm penetration into the sample.

High-resolution microscopy has also shown an extended heat effect on sample surface produced from the laser ablation and its extensive effects on the samples.

This study shows the application of the LIBS technique for identifying corrosion within uranium metal by detecting the presence of elemental oxygen, hydrogen, and additionally carbon within a very dense matrix. The compact hand-held LIBS instrument (eye safe system) used with 1532 nm wavelength and 5 mJ/pulse is capable of ablating sub-micrograms of material from a sample surface, performing 2D rastering, and acquiring broad band spectra from 190-950 nm. These features make this hand-held instrument amenable to detect oxygen and hydrogen, at very low parts-per-million levels, present within materials that are being probed. The study presented here has proven that the technique and testing methodology employed allows characterization of uranium corrosion in a reliable way. The hand-held LIBS instrument allows for rapid analysis of environmentally sensitive materials, with cost reduction in sample transportation, sample preparation, and analysis time.

ACKNOWLEDGEMENTS

Funding for this research was provided by the CNS/Y-12 National Security Complex under the Plant Directed Research and Development program.

Disclaimer and copyright notice

REFERENCES

[1] G. L. Powell, "The Uranium-Hydrogen Binary System," in *Uranium Processing and Properties*, New York, NY, Springer, 2013, pp. 173-188.

[2] N. J. Magnani, "Hydrogen Embrittlement and Stress Corrosion Cracking of Uranium and Uranium Alloys," in *Advances in Corrosion Science and Technology: Volume 6*, Boston MA, Springer, 1976, pp. 89-161.

[3] G. L. Powell, R. K. Schulze and W. J. Siekhaus, "Effect of Hydrogen on Materials," in *International Hydrogen Conference*, 2008.

[4] G. L. Powell, "Metallurgical Technology of Uranium and Uranium Alloys," *ASM,* pp. 877-899, 1981.

[5] A. Loui, "The Hydrogen Corrosion of Uranium: Identification of Underlying Causes and Proposed Mittigation Strategies," LLNL-TR-607653, 2012.

[6] A. Banos, N. J. Harker and T. B. Scott, "A review of urnanium corrosion by hydrogen and the formation of uranium hydride," *Corrosion Science,* vol. 136, pp. 129-147, 2018.

[7] G. L. Powell and J. B. Condon, "Hydrogen in Uranium Alloys," in *Physical Metallurgy of Uranium Alloys*, J.J. Burke, D.A. Colling, A.E. Gorum and J. Greenspan, eds.; Brook Hill, Mass., 1975, pp. 427-461.

[8] E. Garlea, H. Choo, G. Y. Wang, P. K. Liaw, B. Clausen, D. W. Brown, J. Park, P. D. Rack and E. A. Kenik, "E. Garlea, H. Choo, G.Y. Wang, P.K. Liaw, B. Clausen, D.W. Brown, J. Park, P.D. Rack, E.A. Kenik, Hydride-Phase Formation and its Influence on Fatigue Crack Propagation Behavior in a Zircaloy-4 Alloy," *Metallurgical and Materials Transactions A,* vol. 41, no. 11, pp. 2816-2828, 2010.

[9] C. A. Calhoun, E. Garlea, T. Sisneros and S. R. Agnew, "Effects of hydrogen on the mechanical response of α-uranium," *Journal of Nuclear Materials,* vol. 465(Supplement C), pp. 737-745, 2015.

[10] G. L. Powell, "Uranium Corrosion Near Ambient Temperature," in *Uranium Processing and Properties*, New York, NY, Springer, 2013, pp. 189-206.

[11] J. A. Lillard and R. J. Hanrahan Jr, "Corrosion of Uranium and Uranium Alloys," in *ASM Handbooks vol 13B*, ASM International, 2014, pp. 370-384.

[12] J. R. Wachter and D. A. Cremers, "Determination of Uranium in Solution Using Laser-Induced Breakdown Spectroscopy," *Applied Spectroscopy,* vol. 41, no. 6, pp. 1042-1048, 1987.

[13] P. Fichet, P. Mauchien and C. Moulin, "Determination of Impurities in Uranium and Plutonium Dioxides by Laser-Induced Breakdown Spectroscopy," *Appllied Spectroscopy,* vol. 53, no. 9, pp. 1111-1117, 1999.

[14] J. Young, I. M. Botheroyd and A. I. Whitehouse, "Trace Element Analysis of Cast Uranium Metal Using Laser-Induced Breakdown Spectroscopy," in *CLEO/Europe Conference on Lasers and Electro-Optics*, 1998.

[15] I. I. Zherin, S. T. Penin, L. K. Chistyakova and V. I. Kokhanov, "Experimental study of the aerosol formation by hydrolysis of UF6 in gaseous phase under atmospheric conditions," *Journal of Aerosol Science,* vol. 27(SUPPL.1), pp. 0021-8502, 1996.

[16] E. J. Judge, J. M. Berg, L. A. Le, L. N. Lopez and J. E. Barefield, "LIBS Spectral Data for a Mixed Actinide Fuel Pellet Containing Uranium, Plutonium, Neptunium and Americium," Los Alamos National Laboratory Unclassified Report LA-UR 12-22287, Los Alamos, NM, 2012, Pp 1-71.

[17] A. Sarkar, D. Alamelu and S. K. Aggarwal, "A. Sarkar, D. Alamelu, S.K. Aggarwal, Laser-induced breakdown spectroscopy for determination of uranium in thorium–uranium mixed oxide fuel materials," *Talanta,* vol. 78, no. 3, pp. 800-804, 2009.

[18] A. Sarkar, D. Alamelu and S. K. Aggarwal, "Determination of trace constituents in thoria by laser induced breakdown spectrometry," *Journal of Nuclear Materials,* vol. 384, no. 2, pp. 158-162, 2009.

[19] C. A. Smith, M. A. Martinez, D. K. Veirs and D. A. Cremers, "Pu-239/Pu-240 isotope ratios determined using high resolution emission spectroscopy in a laser-induced plasma," *Spectrochimica Acta Part B: Atomic Spectroscopy,* vol. 57, no. 5, pp. 929-937, 2002.

[20] D. A. Cremers, A. Beddingfield, R. Smithwick, R. C. Chinni, C. R. Jones, B. Beardsley and L. Karch, "Monitoring uranium, hydrogen, and lithium and their isotopes using a compact laser-induced breakdown spectroscopy (LIBS) probe and high-resolution spectrometer," *Applied Spectroscopy,* vol. 66, no. 3, pp. 250-261, 2012.

[21] S. S. Harilal, B. E. Brumfield, N. L. LaHaye, K. C. Hartig and M. C. Phillips, "Optical spectroscopy of laser-produced plasmas for standoff isotopic analysis," *Applied Physics Reviews,* vol. 5, no. 021301, 2018.

[22] K. C. Hartig, S. S. Harilal, M. C. Phillips, B. E. Brumfield and I. Jovanovic, "Evolution of uranium monoxide in femtosecond laser-induced uranium plasmas," *Optics Express,* vol. 25, no. 10, pp. 11477-11490, 2017.

[23] R. C. Chinni, D. A. Cremers, L. J. Radziemski, M. Bostian and C. Navarro-Northrup, "R.C. Chinni, D.A. Cremers, L.J. Radziemski, M. Bostian, C. Navarro-Northrup, Detection of Uranium Using Laser-Induced Breakdown Spectroscopy," *Appllied Spectroscopy,* vol. 63, no. 11, pp. 1238-1250, 2009.

[24] A. Sarkar, D. Alamelu and S. K. Aggarwal, "Determination of thorium and uranium in solution by laser-induced breakdown spectrometry," *Applied Optics,* vol. 47, no. 31, pp. G58-G64, 2008.

[25] J. E. Barefield, E. J. Judge, J. M. Berg, S. P. Willson, L. A. Le and L. N. Lopez, "Analysis and spectral assignments of mixed actinide oxide samples using laser-induced breakdown spectroscopy (LIBS)," *Appllied Spectroscopy,* vol. 67, no. 4, pp. 433-440, 2013.

[26] A. M. El Sherbini, H. Hegazy and T. M. El Sherbini, "Measurement of electron density utilizing the Hα-line from laser produced plasma in air," *Spectrochimica Acta Part B: Atomic Spectroscopy,* vol. 61, no. 5, pp. 532-539, 2006.

[27] C. A. Calhoun, E. Garlea, R. P. Mulay, T. A. Sisneros and S. R. Agnew, "Investigation of the effect of thermal residual stresses on deformation of α-uranium through neutron diffraction measurements and crystal plasticity modeling," *Acta Materialia,* vol. 85, pp. 168-179, 2015.

[28] C. A. Calhoun, E. Garlea, T. A. Sisneros and S. R. Agnew, "In-Situ neutron diffraction characterization of temperature dependence deformation in α-uranium," *Journal of Nuclear Materials,* vol. doi: 10.1016/j.jnucmat.2018.01.036., 2018.

[29] E. Garlea, Bridges, R. L., Garlea, V. O., A. D. Carpenter, M. A. Hemphill and J. S. Morrell, "Characterization of a grain size refinement process in cast uranium," *Materials Science & Engineering A,* vol. 559, pp. 210-216, 2013.

[30] B. N. Bennett, M. Z. Martin, D. N. Leonard and E. Garlea, "Calibration Curves for Commercial Copper and Aluminum Alloys Using Handheld," *Applied Physics B,* vol. 124, no. 42, 2018.

[31] SciAps, "LIBS: Handheld Laser Induced Breakdown Spectroscopy (HH LIBS)," LIBS: Handheld Laser Induced Breakdown Spectroscopy (HH LIBS) – SciAps, (2016), [Online]. Available: https://www.sciaps.com/libs-handheld-laser-analyzers/. [Accessed 04 may 2017].

[32] R. S. Harmon, R. R. Hark, C. S. Throckmorton, E. C. Rankey, M. A. Wise, A. M. Somers and L. M. Collins, "Geochemical Fingerprinting by Handheld Laser-Induced Breakdown Spectroscopy," *Geostandards and Geoanalytical Research,* vol. 41, no. 4, pp. 563-584, 2017.

[33] R. Arkush, M. Brill, S. Zalkind, M. H. Mintz and N. Shamir, "The effect of N2+ and C+ implantation on uranium hydride nucleation and growth kinetics," *Journal of Alloys and Compounds,* Vols. 330-332, pp. 472-475, 2002.

[34] M. Balooch and A. V. Hamza, "Hydrogen and water vapor adsoption on and reaction with uranium," *Journal of Nuclear Materials ,* vol. 230, pp. 259-270, 1996.

[35] Z. Z. Wang, Y. Deguchi, M. Kuwahara, T. Taira, X. B. Zhang, J. J. Yan, J. P. Liu, H. Watanabe and R. Kurose, "Quantitative elemental detection of size-segregated particles using laser-induced breakdown spectroscopy," *Spectrochimica Acta Part B: Atomic Spectroscopy,* vol. 87, pp. 130-138, 2013.

[36] M. d. S. Gomes, D. Santos Jr., L. C. Nunes, G. G. A. d. Carvalho, F. d. O. Leme and F. J. Krug, "Evaluation of Grinding Methods for Pellets Preparation Aiming at the Analysis of Plant Materials by Laser Induced Breakdown Spectrometry," *Talanta,* vol. 85, pp. 1744-1750, 2011.

[37] S. S. Harilal, B. E. Brumfield, N. Glumac and M. Phillips, "Elucidating uranium monoxide spectral features from a laser-produced plasma," *Optics Express,* vol. 26, no. 16, pp. 20319-20330, 2018.

[38] E. Tognoni, V. Palleschi, M. Corsi and G. Cristoforetti, "Quantitative micro-analysis by laser-induced breakdown spectrocopy: a review of experimental approaches," *Spectrochimica Acta Part B,* vol. 57, pp. 1115-1130, 2002.

[39] C. Aragón and J. A. Aguilera, "Characterization of laser induced plasma by optical emission spectroscopy: A review of experiements and methods," *Spectrochimica Acta Part B,* vol. 63, pp. 893-916, 2008.

[40] T. C. Totemeier, R. G. Pahl and S. M. Frank, "Oxidation kinetics of hydride-bearing uranium metal corrosion products," *Journal of Nuclear Materials,* vol. 265, pp. 308-320, 1999.

[41] T. C. Totemeier, R. G. Pahl, S. L. Hayes and S. M. Frank, "Characterization of corroded metallic uranium fuel plates," *Journal of Nuclear Materials,* vol. 256, pp. 87-95, 1998.

[42] T. C. Totemeier, "Characterization of uranium corrosion products involved in a uranium hydride pyrophoric event," *Journal of Nuclear Materials,* vol. 278, pp. 301-311, 2000.

[43] J. A. Aguilera and C. Aragón, "Characterization of laser-induced plasma during its expansion in air by optical emission spectroscopy: Observation of strong explosion self-similar behavior," *Spectrochimica Acta Part B,* vol. 97, pp. 86-93, 2014.